

SLAC – PUB – 4025

September 26, 1986

T/E

An Improved Measurement Of the Average
Lifetime of Hadrons Containing Bottom Quarks*

D.E.Klem ^{β ,^(a)} W.B.Atwood ^{β} B.C.Barish ^{α} G.R.Bonneaud ^{γ ,^(b)} A.Courau ^{β ,^(c)} G.J.Donaldson ^{γ ,^(d)}
R.Dubois ^{β ,^(e)} M.M.Duro ^{γ} E.E.Elsen ^{β ,^(f)} S.G.Gao ^{α ,^(g)} Y.Z.Huang ^{α ,^(h)} G.M.Irwin ^{γ}
R.P.Johnson ^{β ,⁽ⁱ⁾} H.Kichimi ^{β ,^(j)} J.Kirkby ^{γ ,^(k)} D.E.Koop ^{α ,^(l)} J.Ludwig ^{α ,^(m)} G.B.Mills ^{α ,⁽ⁿ⁾}
A.Ogawa ^{β} T.Pal ^{α ,^(k)} R.Pitthan ^{β} D.L.Pollard ^{γ ,^(d)} C.Y.Prescott ^{β} L.S.Rochester ^{β}
W.Ruckstuhl ^{α ,^(o)} M.Sakuda ^{α ,^(j)} S.S.Sherman ^{α ,^(p)} R.Stroynowski ^{α} S.Q.Wang ^{β ,^(h)}
S.G.Wojcicki ^{γ} H.Yamamoto ^{α ,^(q)} W.G.Yan ^{γ ,^(h)} C.C.Young ^{β}

^{α} California Institute of Technology, Pasadena, California 91125

^{β} Stanford Linear Accelerator Center, P.O. Box 4349, Stanford, California 94305

^{γ} Physics Department, Stanford University, Stanford, California 94305

(DELCO Collaboration)

Submitted to *Physical Review D*

* This work was supported in part by the Department of Energy, contract numbers DE-AC03-76SF00515 and DE-AC03-81-ER40050, and the National Science Foundation.

ABSTRACT

A measurement of the average lifetime of hadrons containing bottom quarks is presented. The b-hadrons are produced in e^+e^- annihilation at 29 GeV, and the lifetime is determined from the impact parameters of high transverse momentum electrons produced in the decay of the b-hadrons. A b-lifetime of $\tau_b = 1.17_{-0.22}^{+0.27}$ (stat.) $_{-0.16}^{+0.17}$ (sys.) psec is determined from a maximum likelihood fit to the impact parameters. Particular care has been taken to describe the experimental resolution correctly in the fit.

1. Introduction

In the standard model weak decays of hadrons containing bottom quarks indicate the mixing of the b-quark with the lighter d- and s-quarks. This mixing is parameterized by the Kobayashi-Maskawa (K-M) matrix.¹ Because of this, the average lifetime of the b-hadrons provides a constraint on some of the elements of the K-M matrix. The b-lifetime measurement reported here is based on the impact parameter method.² Hadrons containing bottom quarks are identified in hadronic events produced in e^+e^- annihilation by the presence of an electron with a large component of its momentum transverse to the sphericity axis. Because this method of identifying b-decays cannot distinguish between the various b-hadrons (B^+ , B^0 , Λ_b , etc.), this measurement is an average weighted by the unknown production ratios and the unknown semileptonic branching ratios of the various states. While the “average” value of τ_b which is reported here is not necessarily the same “average” measured by experiments which use another method of tagging b-decay,³ this difference is expected to be small.⁴ The present analysis, which supercedes a previous analysis based on a partial dataset,⁵ uses a maximum likelihood fit to estimate the b-lifetime from the impact parameters. Great care has been taken to ensure that the detector resolution is described correctly in this fit. The assumption of a Gaussian shape for the detector resolution, which was used in the previous analysis, has been replaced with a more general description.

The remainder of this paper is divided into seven major sections. The first two provide brief reviews of the DELCO detector and of the analysis of the inclusive electron spectrum. The next section discusses the definition of the impact parameter and the errors affecting its measurement. The following section

describes the maximum likelihood fit used to estimate the b-lifetime as well as several checks done to test the fit. The next section describes a measurement of the tau lifetime performed as a check. The last two sections discuss the systematic errors affecting the b-lifetime and the constraints which this measurement places on elements of the K-M matrix.

2. The Detector

The DELCO detector recorded a total luminosity of 214 pb^{-1} at a center of mass energy of 29 GeV at the PEP e^+e^- storage ring. The detector has been described previously,⁶ and only a brief review of the systems most important to this analysis will be given here. A cross section of the detector is shown in Fig. 1. Charged particle tracks are reconstructed in a system of drift chambers in a magnetic field. This field is produced by two coils and an iron flux return. The field at the center of the detector is 3.3 kG and the total integrated bending strength is 1.8 kG-m. Three separate drift chambers provide a total of 22 layers of tracking. The inner drift chamber (IDC) has six layers in a cylindrical geometry. These layers are located between 12 cm and 20 cm in radius. This chamber achieved a resolution of approximately $170 \mu\text{m}$ on a typical layer. The central drift chamber (CDC) has ten layers which are also arranged in a cylindrical geometry. They are located between 27 cm and 49 cm in radius and achieved a typical resolution of $200 \mu\text{m}$. The planar drift chambers (PDC's) are arranged in a hexagonal geometry at a radius of approximately 1.5 m and achieved a resolution of approximately $450 \mu\text{m}$. This tracking system achieved a momentum resolution of $\frac{\sigma_p}{p} = [(0.02 \cdot p)^2 + (0.06)^2]^{\frac{1}{2}}$, where p is the momentum in GeV.

Particle identification is provided by an atmospheric-pressure Čerenkov counter which is located between the CDC and the PDC's. This counter was run with either isobutane (147 pb^{-1}) or nitrogen (67 pb^{-1}) as a radiator. It provides electron identification at momenta up to the threshold for pions to produce Čerenkov radiation (2.5 GeV in isobutane or 5.5 GeV in nitrogen). The identification provided by the Čerenkov counter is supplemented by information from a system of lead/plastic-scintillator shower counters. These counters are located outside the PDC's. The solid angle covered by both tracking and particle identification is approximately ± 0.62 in $\cos \theta$, where θ is the polar angle.

The position of the beams in the storage ring is determined on an event-by-event basis by two beam position monitors located 3.7 m either side of the interaction point. The errors associated with the beam position monitors are small compared to other errors affecting the tracking.

3. The Electron Analysis

The electron sample used in this analysis was obtained as part of the DELCO inclusive electron analysis and has been described previously.⁷ Only a synopsis of that analysis will be given here. Hadronic events produced in e^+e^- annihilation at 29 GeV are characterized by large multiplicities and large charged energies. In this analysis hadronic events are identified by requiring at least five charged tracks in the event and a total charged energy of at least 6 GeV. In addition each event is divided into two hemispheres according to the sphericity axis, and each hemisphere is required to contain at least two charged tracks. Electrons are identified in these events by the Čerenkov counter in conjunction with the barrel shower counter. The electron analysis includes an explicit requirement that all

tracks have a distance of closest approach to the beam center of less than 0.3 cm. This is necessary in order to reduce the number of electrons from photon conversions in the beam pipe and the inner wall of the IDC. The effect of this cut is explicitly accounted for in the fit to the impact parameters which is described below.

The resulting electron spectrum is fit as a function of the momentum (p) and the momentum transverse to the sphericity axis (p_t) to obtain average semileptonic branching ratios and fragmentation parameters for bottom and charmed quarks. The fit accounts for electrons produced by the semileptonic decay of b-hadrons (b), the decay of b-hadrons into charmed hadrons followed by the semileptonic decay of these charmed hadrons (bc), the semileptonic decay of charmed hadrons produced directly (c), and the various backgrounds (bkg). The backgrounds consist primarily of electrons from photon conversions and misidentified pions. The electron distributions used to fit the data are obtained from a full detector simulation Monte Carlo calculation. The Monte Carlo uses the Lund^{8,9} generator with a modified fragmentation function.¹⁰ The pion background is measured from real hadronic events using a track flipping algorithm.¹¹ A by-product of the fit to the electron spectrum is a model-dependent measurement of the relative contributions of the various sources to the electron signal as a function of p and p_t . These numbers are used in the lifetime analysis.

To display the purity of the electron signal, it is convenient to divide the p, p_t plane into two regions: a “b-region” ($p_t > 1$ GeV) in which most of the tracks are electrons from b-decay, and a “c-region” ($p > 1$ GeV, $p_t < 1$ GeV) in which most of the electrons come from direct c-decay. The contributions to these regions

from the various sources are shown in Table 1. The numbers in this table are calculated from the results of the fit to the electron spectrum. The high purity of the signal in the b-region (the direct and cascade decays of b-hadrons contribute almost 80%) is due to the clean electron identification provided by the Čerenkov counters.

4. Impact Parameters

This analysis, like many previous analyses, uses the impact parameter method.² The impact parameter δ is the distance of closest approach of the track to the nominal beam center. The magnitude and the sign of the impact parameter are calculated in the plane perpendicular to the beams as is shown in Fig. 2. The sign is determined by the point at which the electron track crosses the path of the parent hadron. This is done in a manner such that a positive δ corresponds to the parent hadron traveling a positive distance before decaying. In this analysis the path of the parent hadron is assumed to originate at the center of the beam ellipse, and the direction of the parent hadron is assumed to be along the sphericity axis as determined from all charged tracks in the event.¹² Typical errors due to the latter approximation are about 15° . These errors are caused by the inclusion of charged particles which did not come from the decays of the b-hadrons, by the exclusion of neutral particles produced in the decays, and by gluon radiation.

This definition of δ gives rise to a substantial dependence of the impact parameter on p and p_t . This dependence is displayed in Fig. 3. Because the clean identification of electrons provided by the Čerenkov counter makes it possible to use electrons with momenta as low as 1 GeV, and because the pion threshold in

the Čerenkov counter places an upper limit on the electron momentum of either 2.5 GeV or 5.5 GeV, most of the electrons in the b-region are near the peak in $\bar{\delta}$ shown in Fig. 3. This gives rise to an average impact parameter which, for the same lifetime, is larger than that observed by other experiments.¹³ Additional cuts have been applied to the tracks obtained from the electron analysis. They ensure that the tracks are well measured and minimize the possibility of errors due to confusion between tracks. These cuts consist primarily of requiring that many drift chamber wires are associated with the track, that the residuals after fitting are small, that the z-coordinate of the track origin is consistent with the z-coordinate of the event as determined from all tracks, and that the electron is isolated from all other tracks in the event by at least 50 mrad in ϕ . (The z-axis is parallel to the beams and ϕ is the azimuthal angle.) The result of applying these cuts is to reduce the number of tracks in the b-region from 164 to 113 and the number of tracks in the c-region from 783 to 449. Because the tracks eliminated are predominantly ones which were poorly measured, these cuts have a negligible effect on the statistical significance of the signal. The resulting impact parameter distributions for the b- and c-regions are shown in Fig. 4. The average impact parameter for the b-region is $\bar{\delta} = 259 \pm 49$ (stat.) μm , and for the c-region it is $\bar{\delta} = 146 \pm 28$ (stat.) μm . Both of these numbers are inconsistent with zero by more than five standard deviations.

Two other data sets have been checked for average impact parameters greater than zero. The first of these consists of events from the two-photon process $e^+e^- \rightarrow e^+e^-e^+e^-$. In this case events are selected in which two electrons are tracked in the drift chambers and identified as electrons using the Čerenkov counters. The “parent direction” for these events is taken to be the direction of

the vector sum of the two particles' momenta.¹⁴ The average impact parameter for such tracks, which pass all the tracks quality cuts applied previously and have momentum greater than 1 GeV, is $\bar{\delta} = -0.8 \pm 6.7$ (stat.) μm . This is consistent with zero as expected. The second data set considered consists of all tracks in hadronic events. These tracks are required to pass all of the cuts in the electron analysis except those which specifically deal with the response of the Čerenkov and shower counters.¹⁵ In this case one expects to find an average impact parameter which is greater than zero, but which is small compared to the average impact parameter for electrons from b-decay. This is because a substantial fraction of the tracks in hadronic events come from the decay of long-lived particles. After applying the same track quality cuts which were used above, the average impact parameter of the tracks in the b-region is $\bar{\delta} = 46 \pm 5$ (stat.) μm and in the c-region it is $\bar{\delta} = 42 \pm 2$ (stat.) μm . A full detector simulation Monte Carlo calculation has been done to check that these numbers are consistent with the b-lifetime measured here and with the known value of the charm lifetime.¹⁶ The result of this calculation is $\bar{\delta}_{M.C.} = 38 \pm 11$ (stat.) μm for the b-region and $\bar{\delta}_{M.C.} = 43 \pm 4$ (stat.) μm for the c-region. In both cases the data are consistent with the Monte Carlo calculations.

Because the shapes of the impact parameter distributions shown in Fig. 4 are heavily influenced by the detector resolution, and because a maximum likelihood fit is used to estimate the b-lifetime, care has been taken to understand the errors which affect the measurement of δ . These errors result from the drift chamber resolution, the beam size, and the multiple coulomb scattering in the material in the detector. The width of the "Gaussian core" of the error distribution can be written in the form:

$$\sigma_{\delta}^2 = \sigma_{D.C.}^2 + \sigma_x^2 \cdot \sin^2 \phi + \sigma_y^2 \cdot \cos^2 \phi + \frac{A^2}{p^2 \sin^3 \theta}. \quad (4.1)$$

The first term, $\sigma_{D.C.}$, is the contribution of the drift chamber resolution. The next two terms account for the horizontal (σ_x) and the vertical (σ_y) beam size. The drift chamber resolution and the beam size are measured using tracks from Bhabha events. The results of these measurements are summarized in Table 2 for the various run blocks.¹⁸ The last term in Eq. (4.1) accounts for the multiple scattering in the beam pipe and the drift chambers. The form is motivated by the well known expression for the Gaussian core of the multiple scattering distribution¹⁹ and by the cylindrical geometry of the beam pipe and the drift chambers. The constant A is measured using the electrons from the previously described two-photon events. The results of these measurements are also summarized in Table 2.

The accuracy of this prescription for calculating σ_{δ} , as well as the level of the non-Gaussian tails, can be checked by histogramming the quantity $\frac{\delta}{\sigma_{\delta}}$ for tracks from events with no long-lived particles. This distribution will be referred to as the resolution function P^{rf} . In the simplest case the resolution function would be a Gaussian distribution centered on zero with unit width. The resolution function obtained from Bhabha events is shown in Fig. 5(a) and the resolution function obtained from the two-photon events is shown in Fig. 5(b). In both cases the central core is well approximated by a Gaussian, but there are substantial non-Gaussian tails.

The previous discussion does not account for the degradation in resolution expected in hadronic events. Such a degradation can be caused by confusion between tracks at the track reconstruction stage or by cross-talk in the drift

chambers or associated electronics. It is not possible to address this problem directly by histogramming $\frac{\delta}{\sigma_\delta}$ for tracks from hadronic events. This is because of the large number of K_s 's and Λ 's in these events which populate the tails of the impact parameter distribution and also because of the substantial fraction of these events which contain heavy hadrons. The distribution of $\frac{\delta}{\sigma_\delta}$ for tracks from hadronic events is shown in Fig. 6(a), and the effects of the long-lived particles are clearly evident. These effects have been removed using the unfolding procedure described in the Appendix. The result is shown in Fig. 6(b). The unfolding procedure requires a model for the production and decay of long-lived particles in hadronic events. The same Monte Carlo generator was used for this as was used in the electron analysis. The resolution function obtained from the unfolding procedure has been symmetrized "by hand" to remove a small residual asymmetry which probably reflects an inadequacy in the Monte Carlo calculation of the contribution of long-lived particles to the original distribution. The difference between the symmetrized and the unsymmetrized resolution functions will be included as a systematic error on the final value of the b-lifetime. The resolution function which results from the unfolding is similar to that obtained from the two-photon events, although it has slightly larger tails and is slightly wider. The effect of this difference in resolution on the b-lifetime will also be included as a systematic error. The unfolding is not sensitive to the value of τ_b used in the Monte Carlo.²⁰

In summary, the resolution obtained in measuring the impact parameter is described in the following manner. The quantity σ_δ is calculated for each track from Eq. (4.1). This accounts for the dependence of the resolution on the beam size, the drift chamber resolution, and the multiple scattering. The

errors affecting δ are understood to be distributed according to the symmetrized resolution function (Fig. 6(b)) after this distribution has been scaled to have a width σ_δ .

5. The Fit

This analysis uses a maximum likelihood fit to estimate the b-lifetime. This type of fit makes it possible to account for the substantial differences in resolution from one track to the next and also the substantial variation in $\bar{\delta}$ with p and p_t . It also makes it reasonably straightforward to do a two-parameter fit for both the bottom and charm lifetimes as a check of the fitting procedure. Finally, in a certain sense such fits are the best one can do.²¹ The likelihood function used in this fit has the following form:

$$L = -2 \sum_{i=1}^N \ln \left[f_b^i \cdot P_b^i(\delta) + f_{bc}^i \cdot P_{bc}^i(\delta) + f_c^i \cdot P_c^i(\delta) + f_{bkg}^i \cdot P_{bkg}^i(\delta) \right]. \quad (5.1)$$

In this expression the summation is over the tracks in the fit. The f_x^i 's ($x = b, bc, c, bkg$) are the probabilities that the i th track came from any of the four sources of "electrons" which were enumerated in the section on the electron analysis. The f_x^i 's depend on p and p_t and are obtained from the fit to the electron spectrum. The $P_x^i(\delta)$'s are the impact parameter distributions for the various sources of electrons. They account for the detector resolution and for the effects of long-lived particles. The $P_x^i(\delta)$'s have the form:

$$P_x^i(\delta) = \frac{1}{C} \int_{-\infty}^{\infty} \frac{1}{\sigma_\delta^i} P^{rf} \left(\frac{\delta - \delta'}{\sigma_\delta^i} \right) \cdot \frac{1}{s} P_x^{i,exact} \left(\frac{\delta}{s} \right) d\delta', \quad (5.2)$$

i.e., they are the convolution of two other distributions.²² The first of these, P^{rf} , is the resolution function discussed in the previous section. It is scaled

on a track-by-track basis by σ_b^i . The second of these, $P_x^{i,exact}$, accounts for the influence of particles with finite lifetimes on the impact parameter distribution. These distributions are determined by Monte Carlo calculations for 0.5 GeV square bins in p and p_t . The dependence of these “exact” impact parameter distributions on the relevant lifetime is introduced by scaling the distributions according to $s = \frac{\tau_x}{\tau_o}$, where τ_o is the lifetime for which the distribution was originally generated and τ_x is the desired lifetime. This scaling procedure is used only for P_b^i and P_c^i . It is not necessary for the background distribution since it does not depend on either τ_b or τ_c , and it is not possible for the cascade process because this source of electrons does not have any simple scaling properties. In the latter case the distribution is put into the fit with fixed values of τ_b and τ_c , and then new values of τ_b and τ_c are determined from the data and new distributions generated. Since the contribution to the signal from this process is a relatively small part of the total, this procedure converges quickly. The factor of $\frac{1}{C}$ in Eq. (5.2) is calculated so that the normalization is preserved, *i.e.*,

$$\int_{-\infty}^{\infty} P_x^i(\delta) d\delta = 1. \quad (5.3)$$

This is necessitated by the $\delta_{max} = 0.3$ cm maximum impact parameter cut. Because of the small backgrounds in the b-region, the overall systematic uncertainty on the b-lifetime is minimized by fitting just the tracks in this region. The loss of statistical precision resulting from not including the tracks in the c-region in the fit is small (see below). The result of such a fit (with τ_c fixed to 0.64 psec^{16}) is $\tau_b = 1.17_{-0.22}^{+0.27}$ (stat.) psec.

Numerous checks have been performed to verify that the fit has been done

properly. The result of a two-parameter fit to all the tracks in both the b- and c-regions is shown in Fig. 7. This figure is a contour plot of L as a function of τ_b and τ_c . It has a minimum at $\tau_b = 1.12_{-0.21}^{+0.24}$ (stat.) psec and $\tau_c = 0.81_{-0.24}^{+0.24}$ (stat.) psec. This value of τ_c is consistent with previous measurements which average to $\tau_c = 0.64$ psec.¹⁶

In Fig. 4 the smooth curves are the result of a Monte Carlo calculation of the impact parameter distributions for the two regions. These calculations are based on $\tau_b = 1.17$ psec and $\tau_c = 0.64$ psec, and were calculated using the impact parameter distributions and the detector resolution used in the fit. The means of these distributions, $\bar{\delta}_{M.C.} = 222 \pm 6$ (stat.) μm for the b-region and $\bar{\delta}_{M.C.} = 101 \pm 3$ (stat.) μm for the c-region, are consistent with the data.²³ It is clear from the figures that the number of particles in the tails of the data is consistent with the number of particles expected. The χ^2 's for these figures have been calculated²⁴ and are 7.1 for 7 degrees of freedom for the b-region and 6.6 for 10 degrees of freedom for the c-region. In both cases the data are consistent with the Monte Carlo calculations.

Another goodness of fit test uses the value of the function L at its minimum. In the case of a Gaussian distribution, L_{min} is simply related to χ^2 by

$$\chi^2 = L_{min} - \sum_{i=1}^N \log(2\pi\sigma_i^2).$$

In the present case the distributions are not Gaussian, but it is possible to define a similar quantity, " χ^2 ", by an analogous expression. The expected distribution of " χ^2 " for the one parameter fit has been obtained from a Monte Carlo calculation and is shown in Fig. 8 along with the value obtained from the data. The value

of “ χ^2 ” obtained from the data is consistent with the Monte Carlo calculation at the 84% confidence level.²⁵

Two more tests can be done by introducing free parameters into the fit. In the first case a parameter, ϵ , is introduced which scales all of the errors in the fit, *i.e.*, $\sigma_\delta \rightarrow \epsilon \cdot \sigma_\delta$. For its nominal value of $\epsilon = 1.0$, the fit reduces to the previous case. By leaving ϵ a free parameter in the fit, some sensitivity is obtained to errors in the overall scale of the σ_δ 's. Fig. 9 shows a contour plot of the likelihood function versus τ_b and ϵ . The fitted values of $\tau_b = 1.27$ psec and $\epsilon = 0.81$ are consistent with $\tau_b = 1.17$ psec and with the nominal value of ϵ . A similar test involving the introduction of a flat background into the fit has also been done. It yields a value of the flat background consistent with zero.²⁶

The last test that will be described takes advantage of the fact that the δ_{max} cut is explicitly accounted for in the fit. Because of this, the measured b-lifetime can be plotted easily as a function of δ_{max} . This is shown in Fig. 10. The “sawtooth” shape can be understood as follows. As δ_{max} is made smaller, the correction to τ_b increases. This gives rise to the slope of the curves. At distinct values of δ_{max} particular tracks are dropped from the fit. This results in the discontinuities. Because the gradual changes offset the discontinuities, this figure provides additional evidence that the fit is not being pulled by the tails of the data.²⁷

6. The Tau Lifetime

An analysis similar to that of the b-lifetime has been done to measure the lifetime of the tau lepton. Since this lifetime has been measured previously with high precision,²⁸ and since the tau events suffer from tracking confusion problems which are similar to those in hadronic events, this analysis serves as a useful check on the b-lifetime measurement. Because taus decay predominantly into either one or three charged particles, tau pairs produced in e^+e^- annihilation at $E_{\text{cm}} = 29$ GeV have a clean signature in the form of events with one charged track recoiling against three charged tracks. In such events the large velocity of the taus in the laboratory frame ($\gamma \approx 8$) results in very clear separation of the decay products from the two taus. The cuts primarily responsible for identifying these events are as follows. Each event is required to have four well measured tracks whose charge sums to zero. The charged energy of each event is required to be between 6 and 24 GeV and the thrust greater than 0.97. Each event must have three tracks in one hemisphere of the event and one track in the other.²⁹ The three track side of the event must have a charged energy of at least 3 GeV and an invariant mass consistent with a tau decay.

The result of these cuts is a data set of 1357 events. Monte Carlo calculations indicate that there should be backgrounds of 31 hadronic events and 12 Bhabha events. The latter arise from radiative Bhabha events in which the photon converts to produce an electron-positron pair. Both of these backgrounds are negligible compared to the statistical uncertainty of the final answer and are neglected in what follows. After applying the same track quality cuts used in the electron analysis and requiring a momentum of at least 1 GeV, there are 2177 tracks. The impact parameter distribution for these tracks is shown in Fig. 11.

The mean of this distribution is $\bar{\delta} = 56.8 \pm 9.3$ (stat.) μm . This number can be related to the tau lifetime by a simple Monte Carlo calculation. The result of such a calculation is $\bar{\delta}_{M.C.} = (3.2 \pm 7.7)\mu\text{m} + \left[(204 \pm 21) \frac{\mu\text{m}}{\text{psec}} \right] \cdot \tau_\tau$, where the errors are from the limited statistics of the Monte Carlo calculation.³⁰ This implies a lifetime of $\tau_\tau = 0.26 \pm 0.05$ (stat.) psec.

It is also possible to estimate the tau lifetime by a maximum likelihood technique similar to that used to estimate the b-lifetime. In this case the fit is simplified somewhat because there is only one source of tracks. The fit is done as a function of the tau lifetime and ϵ . The parameter ϵ was introduced previously and scales all the errors in the fit. A contour plot of the likelihood function in the τ_τ, ϵ plane is shown in Fig. 12. The value of ϵ obtained here, $\epsilon = 0.96 \pm 0.02$, is not inconsistent with the nominal value of 1.0.³¹ Since this fit uses the resolution function obtained from the hadronic events, and since the multiplicities in tau events are somewhat lower than in hadronic events, it is reasonable that the resolution in the tau events might be slightly better than that in the hadrons. The value of the tau lifetime obtained from this fit is $\tau_\tau = 0.30_{-0.04}^{+0.05}$ (stat.) psec.³² Both this value and the value inferred from $\bar{\delta}$ are consistent with the “known value” of $\tau_\tau = 0.286 \pm 0.016$ (stat.) ± 0.025 (sys.) psec.²⁸

7. Systematic Errors

There are two major sources of systematic error in this analysis. The first arises from the limited statistics of the electron analysis, and the second from the uncertainty in the resolution function used in the fit. In addition to these sources of uncertainty, there is a minor error introduced into the analysis by the modeling of the sphericity axis in the Monte Carlo calculations. The uncertainty associated with this is estimated to be $^{+0.03}_{-0.00}$ psec. The value of τ_b obtained from the fit is insensitive to the average charm lifetime used.³³

The limited statistics of the electron analysis introduce uncertainties into the b-lifetime analysis by two routes.³⁴ The first of these is by way of the relative contributions of the various sources of electrons (the f_x 's in Eq. (5.1)). The second is by way of the fragmentation functions used in the generation of the exact impact parameter distributions used in the fit. The fragmentation functions have been adjusted to produce the same mean value of $z = \frac{E_{hadron}}{E_{beam}}$ as is observed in the data. The correlations between these errors are known from the electron analysis and have been taken into account in determining the uncertainty on τ_b . The result of this calculation is that this systematic error is dominated by the uncertainty in the b-quark fragmentation. This contributes an uncertainty to τ_b of $^{+0.07}_{-0.12}$ psec.³⁵

The second major source of systematic uncertainty in this analysis is the detector resolution. The resolution function used in the fit was obtained by symmetrizing the resolution function unfolded from the hadrons. The result of fitting the data with the unsymmetrized resolution function is a value of τ_b which is 0.04 psec smaller than the nominal value of $\tau_b = 1.17$ psec. The value of τ_b obtained using the resolution function from the two-photon events is 0.07

psec greater than the nominal value. This is included as a systematic error to account for the small possibility that the degradation in resolution observed in the hadronic events does not affect the electrons. A conservative estimate of the total systematic error is obtained by adding linearly all the systematic errors listed above. The result of this is ${}^{+0.17}_{-0.16}$ psec.

8. Conclusions

A measurement of the average lifetime of hadrons containing bottom quarks has been presented. It is based on a sample of 113 high p_t electrons produced in e^+e^- annihilation at a center of mass energy of 29 GeV. The value of τ_b obtained from a maximum likelihood fit to the impact parameters of these tracks is

$$\tau_b = 1.17 \begin{matrix} +0.27 \\ -0.22 \end{matrix} \text{ (stat.) } \begin{matrix} +0.17 \\ -0.16 \end{matrix} \text{ (sys.) psec.}$$

This value of τ_b is consistent with a recent world average.³⁶ The fit used here accounts for the various non-b-decay sources of tracks in the data sample, the non-Gaussian tails on the detector resolution, and the ± 0.3 cm maximum impact parameter cut.

This measurement can be used to put constraints on elements of the K-M matrix.¹ This matrix describes the mixing of the various generations of quarks. Various calculations have been presented which relate the experimentally observed decay rates to elements of this matrix.^{37,38} The calculation used here^{39,40} is based on a constituent-quark model. It predicts a total decay rate of

$$\frac{1}{\tau_b} = \Gamma = \frac{1}{\text{BR}(b \rightarrow eX)} \cdot [0.58 \cdot |V_{cb}|^2 + 1.18 \cdot |V_{ub}|^2] \cdot 10^{14} \text{ sec}^{-1}, \quad (8.1)$$

where $\text{BR}(b \rightarrow eX)$ is the bottom quark semileptonic branching ratio. The

most precise single measurement of this is $\text{BR}(b \rightarrow eX) = 0.12 \pm 0.007$ (stat.) ± 0.005 (sys.).⁴¹ The constraints placed on $|V_{cb}|$ and $|V_{ub}|$ by this measurement of τ_b are shown in Fig. 13. Also shown in this figure is a constraint on the non-charm branching fraction obtained from the endpoint of the lepton spectrum in b-decay.⁴² From this figure it is clear that the $b \rightarrow u$ transition makes a small contribution to the total rate. If this contribution is neglected entirely, then $|V_{cb}|$ is constrained to be

$$|V_{cb}| = 0.042 \begin{matrix} +0.005 \\ -0.004 \end{matrix} \text{ (stat.)} \begin{matrix} +0.004 \\ -0.002 \end{matrix} \text{ (sys.)}$$

where the systematic error reflects only the systematic uncertainty associated with τ_b and not any uncertainty associated with Eq. (8.1).

9. Acknowledgements

We wish to acknowledge the contributions to DELCO by the technical staffs of Caltech, SLAC Group A, SLAC Group G, and the PEP Division. A.C. and G.B. thank the French National Scientific Research Center, and E.E. the A. v. Humboldt Foundation. This work was supported in part by the Department of Energy, under Contract numbers DE-AC03-76SF00515 and DE-AC03-81-ER40050, and the National Science Foundation.

APPENDIX

This appendix contains a brief description of the unfolding procedure used to obtain the resolution function from the distribution of $\frac{\delta}{\sigma_\delta}$ for tracks in hadronic events. The procedure used here is similar to one described previously.⁴³ The predicted distribution of $\frac{\delta}{\sigma_\delta}$ in the data is given by

$$P_i = \int_{-\infty}^{\infty} P^{rf}(y) \cdot C_i(y) dy. \quad (1)$$

P_i is the probability that $\frac{\delta}{\sigma_\delta}$ for a track in a hadronic event will fall into the i th bin. The functions $C_i(y)$ describe the probability that a track which would have had $\frac{\delta}{\sigma_\delta}$ in the interval $[y, y + dy]$ will, because of long-lived particles, have a $\frac{\delta}{\sigma_\delta}$ which falls into the i th bin. Because the relevant lifetimes are known, the $C_i(y)$'s are known functions. The resolution function, $P^{rf}(y)$, is represented by a sum of other functions:

$$P^{rf}(y) = \sum_{j=1}^{20} a_j \cdot p_j(y). \quad (2)$$

The $p_j(y)$'s are cubic b-splines as suggested in Ref. 43. These functions are shown in Fig. 14. The a_j 's are constants to be determined from the data. Substituting P^{rf} from Eq. (2) into Eq. (1) and interchanging the order of integration and summation makes it possible to write

$$P_i = \sum_{j=1}^{20} C_{ij} \cdot a_j \quad (3)$$

where

$$C_{ij} = \int_{-\infty}^{\infty} p_j(y) \cdot C_i(y) dy. \quad (4)$$

Because the C_{ij} 's depend only on the b-splines and the $C_i(y)$'s, they can be

obtained from a Monte Carlo calculation. It is then straightforward to estimate the values of the a_j 's by fitting the P_i 's to the measured data. The unfolded resolution function shown in Fig. 6(b) is obtained by integrating Eq. (2) over the relevant bins and then symmetrizing the result.⁴⁴

- (a) Present address: Department of Physics, Carlton University, Ottawa, Ontario K1S 5B6, Canada.
- (b) Present address: L.P.N.H.E., Ecole Polytechnique, Route de Saclay, F-91128 Palaiseau, France.
- (c) Present address: Laboratoire de l'Accélérateur Linéaire, Centre d'Orsay, Bat. 200 F-91405, Orsay CEDEX, France.
- (d) Present address: Watkins-Johnson Co., 2525 North First Street, San Jose, CA 95131-1097.
- (e) Present address: Department of Physics, University of Victoria, P.O. Box 1700, Victoria, B.C. V8W 2Y2, Canada.
- (f) Present address: DESY, F-22, Notkestrasse 85, D-2000 Hamburg 52, West Germany.
- (g) Present address: Department of Physics, Beijing University, Beijing, The People's Republic of China.
- (h) Present address: Institute of High Energy Physics, P.O. Box 918, Beijing, The People's Republic of China.
- (i) Present address: Department of Physics, University of Wisconsin, Madison, Wisconsin 53706.
- (j) Present address: National Lab. for High Energy Physics, KEK, Oho-machi, Tsukuba-gun, Ibaraki-ken, 305 Japan.
- (k) Present address: CERN, EP-Division, CH-1211, Geneva 23, Switzerland.
- (l) Present address: Spectra Physics, 3333 North 1st St, San Jose, Ca. 95134-1995.

- (*m*) Present address: Fakultät für Physik, Albert-Ludwigs-Universität, Hermann-Herder Strasse 3, 7800 Freiburg, West Germany.
- (*n*) Present address: Department of Physics, University of Michigan, Ann Arbor, Michigan 48109.
- (*o*) Present address: Department of Physics, University of Geneva, 24 quai E. Ansermet, CH-1211 Geneva 4, Switzerland.
- (*p*) Deceased.
- (*q*) Present address: Enrico Fermi Institute, University of Chicago, 5640 Ellis Ave., Chicago, Ill. 60637.

REFERENCES

1. M. Kobayashi and T. Maskawa, *Prog. Theor. Phys.* **49**, 652 (1973).
2. This method has been used previously. See, for instance, W. Bartel *et al.*, *Phys. Lett.* **114B**, 71 (1982); N. S. Lockyer *et al.*, *Phys. Rev. Lett.* **51**, 1316 (1983); or E. Fernandez *et al.*, *Phys. Rev. Lett.* **51**, 1022 (1983).
3. As an example see M. Althoff *et al.*, *Phys. Lett.* **149B**, 524 (1984).
4. J. Jaros, in *Proceedings of Physics in Collision 4*, edited by A. Seiden (Editions Frontières, Gif sur Yvette, France, 1984), p.257.
5. D. E. Klem *et al.*, *Phys. Rev. Lett.* **53**, 1873 (1984).
6. J. Kirkby, *J. Phys.(Paris), Colloq.* **43**, C3-45 (1982); G. Gidal *et al.* (Berkeley Particle Data Group), Lawrence Berkeley Laboratory Report No. LBL-91, Suppl. UC-37, 1983 (unpublished).
7. T. Pal *et al.*, *Phys. Rev. D* **33**, 2708 (1986).
8. T. Sjostrand, *Comput. Phys. Commun.* **27**, 243 (1982).
9. T. Sjostrand, *Comput. Phys. Commun.* **28**, 229 (1983).
10. C. Peterson *et al.*, *Phys. Rev. D* **27**, 105 (1983).
11. D. E. Koop *et al.*, *Phys. Rev. Lett.* **52**, 970 (1984); D. E. Koop, Ph.D. thesis, California Institute of Technology Report No. CALT-68-1149, 1984 (unpublished).
12. The sphericity axis is taken to point into the same hemisphere as the electron track.
13. See, for example, the papers listed in Ref. 2.
14. From the definition of the impact parameter given above, it is clear that it is not possible to produce an average impact parameter different from zero

unless there exists a correlation between the impact parameter and the assumed parent direction. The value of $\bar{\delta}$ obtained from the two-photon events demonstrates the difficulty of generating such correlations.

15. Examples of such cuts would be the requirement that the Čerenkov cell occupied by the track in question not contain any other tracks with momentum greater than pion threshold or that there not be any track stubs in the PDC's behind the Čerenkov cell.
16. The following fractions, semi-electronic branching ratios, and lifetimes have been used: D^0 53%, 5%, 0.44 psec; D^+ 27%, 16%, 0.92 psec; F^+ 13%, 10%, 0.19 psec; charmed baryons 7%, 5%, 0.23 psec. They produce an average charm lifetime of 0.64 psec. These lifetimes are taken from C. Wohl *et al.*, Rev. Mod. Phys. **56**, s1 (1984).
17. H. Yamamoto *et al.*, Phys. Rev. **D 32**, 2901 (1985).
18. The contributions to the resolution from the beam size and the drift chamber resolution are separated to highlight the origin of these errors. In fact the quantities which are most easily measured and which are used in the analysis are $\sigma_{D.C.}^2 + \sigma_x^2$ and $\sigma_{D.C.}^2 + \sigma_y^2$. The drift chamber resolution, $\sigma_{D.C.}$, is measured from the two-track separation near the origin in Bhabha events and has been subtracted off to get the numbers in the table. The numbers presented here differ slightly from those given in previous publications.^{5,17} These changes are due to differences in the run blocks used, changes in the detector calibrations, and changes in the procedures used to measure the resolution.
19. C. Wohl *et al.*, Rev. Mod. Phys. **56**, s1 (1984).

20. Changing the value of τ_b used in the unfolding by a factor of 2 produces a negligible change in the value of τ_b obtained from the fit.
21. M. Kendall and A. Stuart, *The Advanced Theory of Statistics, Volume 2, Inference and Relationship* (Macmillan, New York, 1979) p. 39.
22. The factors of $\frac{1}{\sigma_b^2}$ and $\frac{1}{s}$ are needed to maintain the normalization of P^{rf} and $P_x^{i,exact}$, respectively.
23. Average impact parameters calculated for the b- and c-regions with a full detector simulation Monte Carlo also yield consistent results.
24. The χ^2 's are calculated according to $\sum \frac{(N_{data} - N_{M.C.})^2}{N_{M.C.}}$ where the sum is only over bins where $N_{data} \neq 0$. The number of degrees of freedom is taken to be the number of bins minus 1 (b-region) or the number of bins (c-region).
25. That is, 84% of the time one would expect a worse fit.
26. More details may be found in D. E. Klem, Ph.D. thesis, SLAC-Report-300, 1986 (unpublished).
27. As δ_{max} is made smaller, the statistical uncertainty on τ_b increases. At $\delta_{max} = 0.2$ cm this uncertainty is ${}^{+0.32}_{-0.27}$ psec and at $\delta_{max} = 0.1$ cm it is ${}^{+0.70}_{-0.43}$ psec.
28. J. A. Jaros, in *Proceedings of the 1984 SLAC Summer Institute* edited by Patricia M. McDonough, SLAC-281, p.427.
29. The event is divided into two hemispheres using the thrust axis.
30. For τ_r in the range of 0.2 to 0.4 psec, the statistical uncertainty on $\bar{\delta}_{M.C.}$ due to the limited statistics of the Monte Carlo is less than 5 μm . Because of correlations between the errors, this is smaller than what would be inferred from the expression in the text. This uncertainty is small compared to the

statistical uncertainty on $\bar{\delta}$ in the data.

31. A change of ϵ from 1.0 to 0.96 would change the fitted b-lifetime by only 0.02 psec.
32. The result of fixing ϵ to 1.0 in this fit is $\tau_\tau = 0.25^{+0.04}_{-0.04}$ (stat.) psec. This is also consistent with the known value.
33. Allowing τ_c to vary over $0.64^{+0.10}_{-0.08}$ psec changes the fitted value of τ_b by less than 0.01 psec.
34. In the electron analysis systematic errors were taken into account by introducing additional parameters into the fit. Because the b-lifetime analysis is only sensitive to the ratio of the f_x 's in Eq. (5.1), some of the systematic uncertainties which affect the electron analysis (i.e., the uncertainty in the luminosity) do not affect the b-lifetime analysis. Other systematic errors do introduce small uncertainties. These errors are included in the $^{+0.07}_{-0.12}$ psec uncertainty attributed to the electron analysis.
35. The value of \bar{z}_b from the fit to the electron spectrum is 0.72. The quoted systematic error corresponds to an uncertainty of ± 0.05 on \bar{z}_b .
36. E. Thorndike, *Ann. Rev. Nucl. Part. Sci.* **35**, 195(1985).
37. M. Gaillard and L. Maiani, in *Proceedings of the 1979 Cargèse Summer Institute on Quarks and Leptons*, edited by M. Levy *et al.* (Plenum, New York, 1979), p. 433.
38. J. Lee-Franzini, in *European Topical Conference on Flavor Mixing in Weak Interactions*, edited by Ling-Lie Chau (Plenum, New York, 1985), p.217.
39. B. Grinstein *et al.*, *Phys. Rev. Lett.* **56**, 298 (1986).

40. B. Grinstein *et al.*, California Institute of Technology - University of Toronto Report No. CALT-68-1311, UTPT-85-37, 1985 (unpublished).
41. A. Chen *et al.*, Phys. Rev. Lett. **52**, 1084 (1984).
42. $\Gamma(b \rightarrow ue\bar{\nu}_e) / \Gamma(b \rightarrow ce\bar{\nu}_e) < 9\%$ is reported in Ref. 36.
43. V. Blobel, DESY Report No. 84-118, 1984 (unpublished).
44. By symmetrizing one means $P^{rf}(y) \rightarrow 0.5 \cdot (P^{rf}(y) + P^{rf}(-y))$.

FIGURE CAPTIONS

1. A cross section of the DELCO detector. Charged particle tracking is provided by three sets of drift chambers in a magnetic field. Electrons are identified by a system of gas Čerenkov counters and a system of lead/plastic-scintillator shower counters.
2. The definition of the impact parameter. This figure lies in the plane perpendicular to the beams. A b-hadron is produced at the point marked primary vertex. In this figure the b-hadron is shown decaying into three charged tracks. Tracks one and three intersect the sphericity axis at spots which correspond to the b-hadron having traveled a positive distance from the center of the beam ellipse before decaying, and they therefore have $\delta > 0$. Track two has $\delta < 0$. In this figure this arises because the primary vertex is not coincident with the center of the beam ellipse. Impact parameters less than zero are also produced by tracking errors and because the sphericity axis may not reflect the true direction of the b-hadron.
3. The average impact parameter as a function of p and p_t for electrons from the decay of b-hadrons. This figure is the result of a Monte Carlo calculation with $\tau_b = 1.0$ psec. The dashed line shows the $p = p_t$ limit.
4. The impact parameter distribution for the b-region (a) and the c-region (b) defined in the text. The points are the data and the smooth curves are the expected distributions based on $\tau_b = 1.17$ psec and $\tau_c = 0.64$ psec. Both distributions are clearly shifted in the direction of positive impact parameters as is expected in the presence of long-lived particles.
5. The distribution of $\frac{\delta}{\sigma_\delta}$ for tracks from Bhabha events (a) and two-photon

events (b). In these figures the histogram is the data and the smooth curve is a Gaussian distribution with a mean of zero and a width of unity included for purposes of comparison. In both cases the data agree well with the Gaussian distribution inside of about ± 2 standard deviations, but there are significant non-Gaussian tails outside of this region. These tails are taken into account in the fit. (See the text.)

6. The distribution of $\frac{\delta}{\sigma_b}$ for tracks in hadronic events (a) and the same distribution after correcting for the long-lived particles in these events (b). In these figures the histogram is the data and the smooth curve is a Gaussian distribution with a mean of zero and a width of unity included for purposes of comparison. The distribution in part (b) is obtained from the unfolding procedure described in the text. The maximum likelihood fit for the b-lifetime uses the distribution in part (b) as a description of the detector resolution.
7. The result of a two-parameter fit for the bottom (τ_b) and the charm (τ_c) lifetimes. All electron tracks with $p > 1$ GeV are used in this fit. The figure is a contour plot of L (see Eq. (5.1)) versus τ_b and τ_c . The minimum of L occurs at $\tau_b = 1.12$ psec and $\tau_c = 0.81$ psec. Contours are shown at the one, two, and three σ levels. The values of τ_b and τ_c obtained from this fit are consistent with the value of τ_b obtained from the one parameter fit and with previous measurements of τ_c .
8. The distribution of " χ^2 " expected for the one-parameter fit to the tracks in the b-region. (See the text for the definition of " χ^2 ".) The distribution shown here is the result of a Monte Carlo calculation. The small arrow shows the value of " χ^2 " obtained from the fit. The value obtained is

consistent with the Monte Carlo calculation.

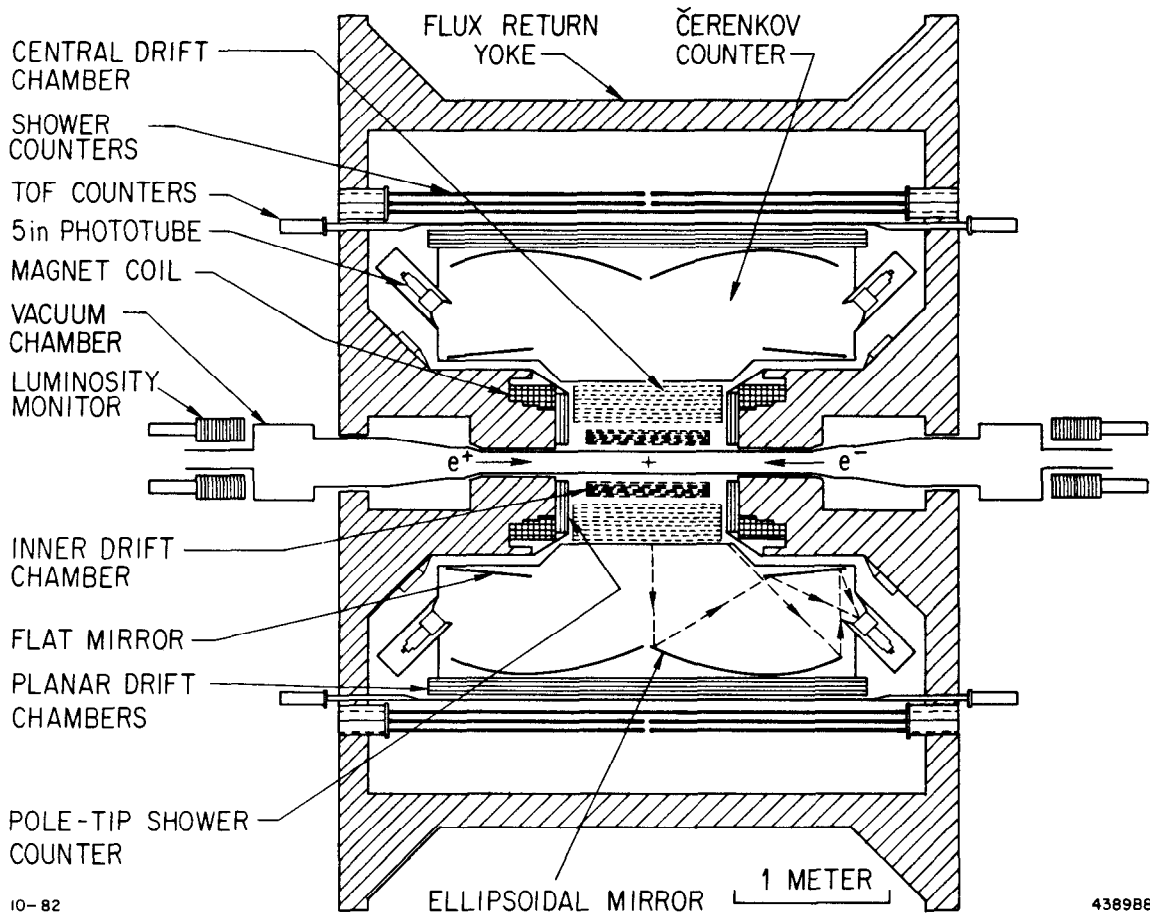
9. The result of a two-parameter fit for the bottom lifetime (τ_b) and the parameter which expands the errors used in the fit (ϵ). This plot uses only the data in the b-region. The figure is a contour plot of L (see Eq. (5.1)) versus τ_b and ϵ . Contours are shown at the one, two, and three σ levels. The value of ϵ obtained is consistent with the nominal value of $\epsilon = 1$.
10. The fitted b-lifetime (τ_b) versus the largest impact parameter used in the fit (δ_{max}). The shape of the curve is explained in the text.
11. The impact parameter distribution from tracks from tau decays. The points are the data and the smooth curve is a Monte Carlo calculation based on a tau lifetime of 0.3 psec.
12. The result of a two-parameter fit for the tau lifetime (τ_τ) and the parameter which expands the errors (ϵ). The minimum occurs at $\tau_\tau = 0.30_{-0.04}^{+0.05}$ (stat.) psec and $\epsilon = 0.96_{-0.02}^{+0.02}$ (stat.). Contours are shown at the one, two, and three σ levels.
13. Constraints on $|V_{ub}|$ and $|V_{cb}|$. The solid curved line comes from $\tau_b = 1.17$ psec. The dashed lines near it are the limits due to the statistical errors. The dotted lines are the limits due to adding the statistical and systematic errors linearly. The solid straight line comes from a limit on the ratio $\frac{\Gamma(b \rightarrow ue\bar{\nu}_e)}{\Gamma(b \rightarrow ce\bar{\nu}_e)} < 9\%$ (90% confidence limit).⁴¹
14. The twenty cubic b-splines used in the unfolding of the resolution function. Each spline is a single “bump” extending over a finite interval.

TABLE CAPTIONS

1. The fractions of tracks from various sources for the b-region and the c-region defined in the text. These numbers are obtained as part of the fit to the electron spectrum.
2. A summary of the resolution obtained for three separate run blocks. Eq. (4.1) expresses the total error on the impact parameter in terms of the quantities in this table. The contribution from the drift chamber resolution is given by $\sigma_{D.C}$, the horizontal and the vertical beam sizes are given by σ_x and σ_y respectively, and the multiple scattering contribution for a 1 GeV track is given by A .

region	b	bc	c	bkg
b	0.70	0.09	0.17	0.04
c	0.15	0.15	0.56	0.14

run block	$\sigma_{D.C.}$ (μm)	σ_x (μm)	σ_y (μm)	A ($\mu\text{m} \cdot \text{GeV}$)
#1	212^{+3}_{-3}	459^{+7}_{-7}	0^{+68}_{-0}	246^{+4}_{-4}
#2	241^{+2}_{-2}	367^{+4}_{-4}	22^{+24}_{-22}	263^{+2}_{-2}
#3	220^{+1}_{-1}	320^{+4}_{-4}	56^{+9}_{-10}	198^{+2}_{-2}



10-82

438986

Fig. 1

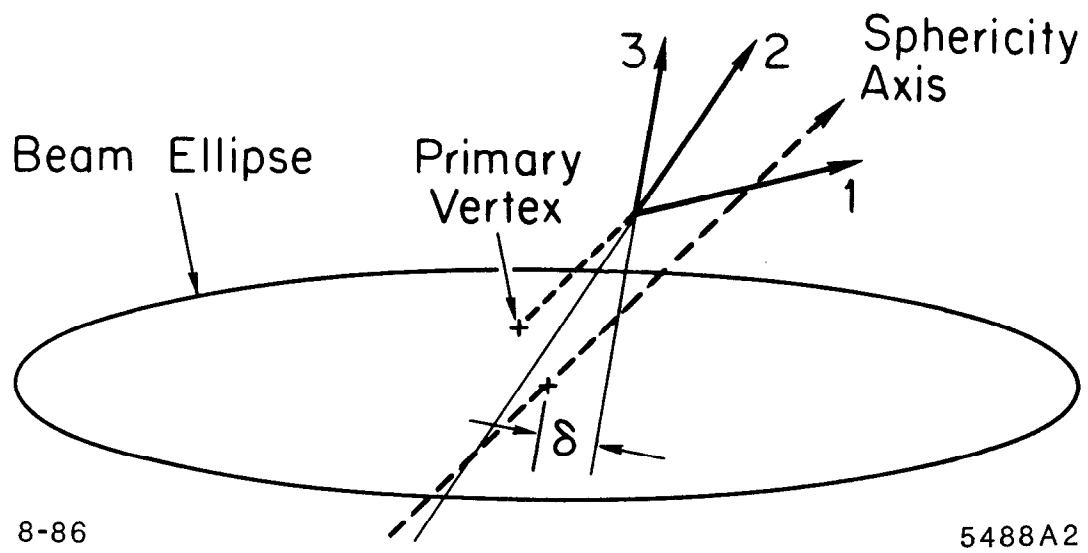


Fig. 2

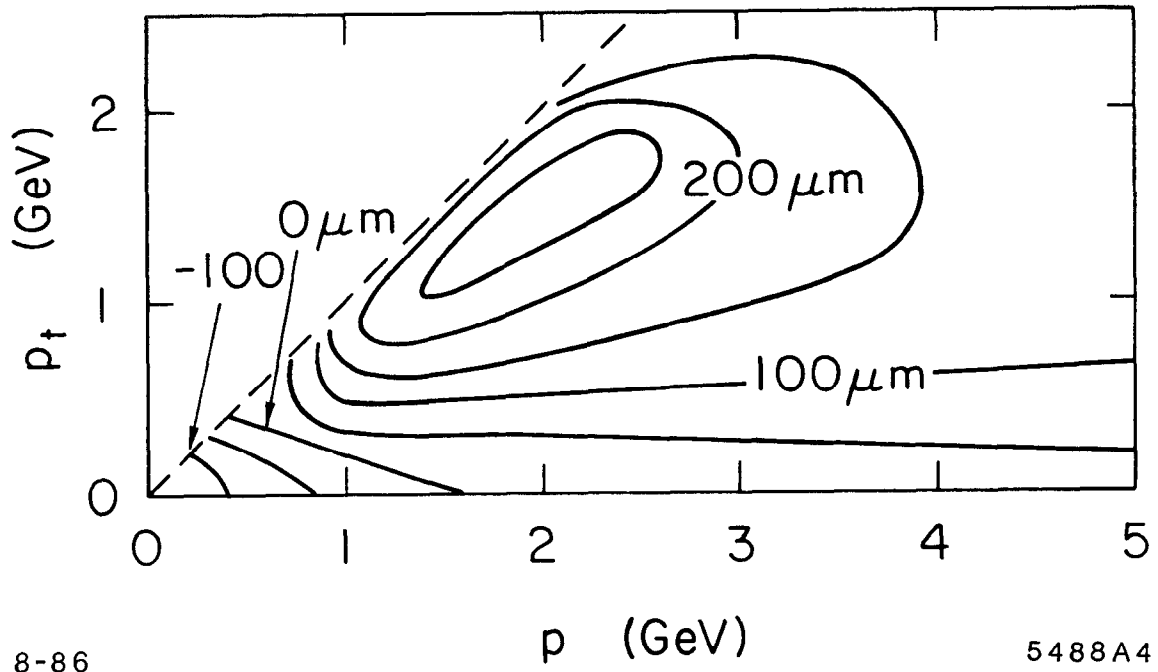
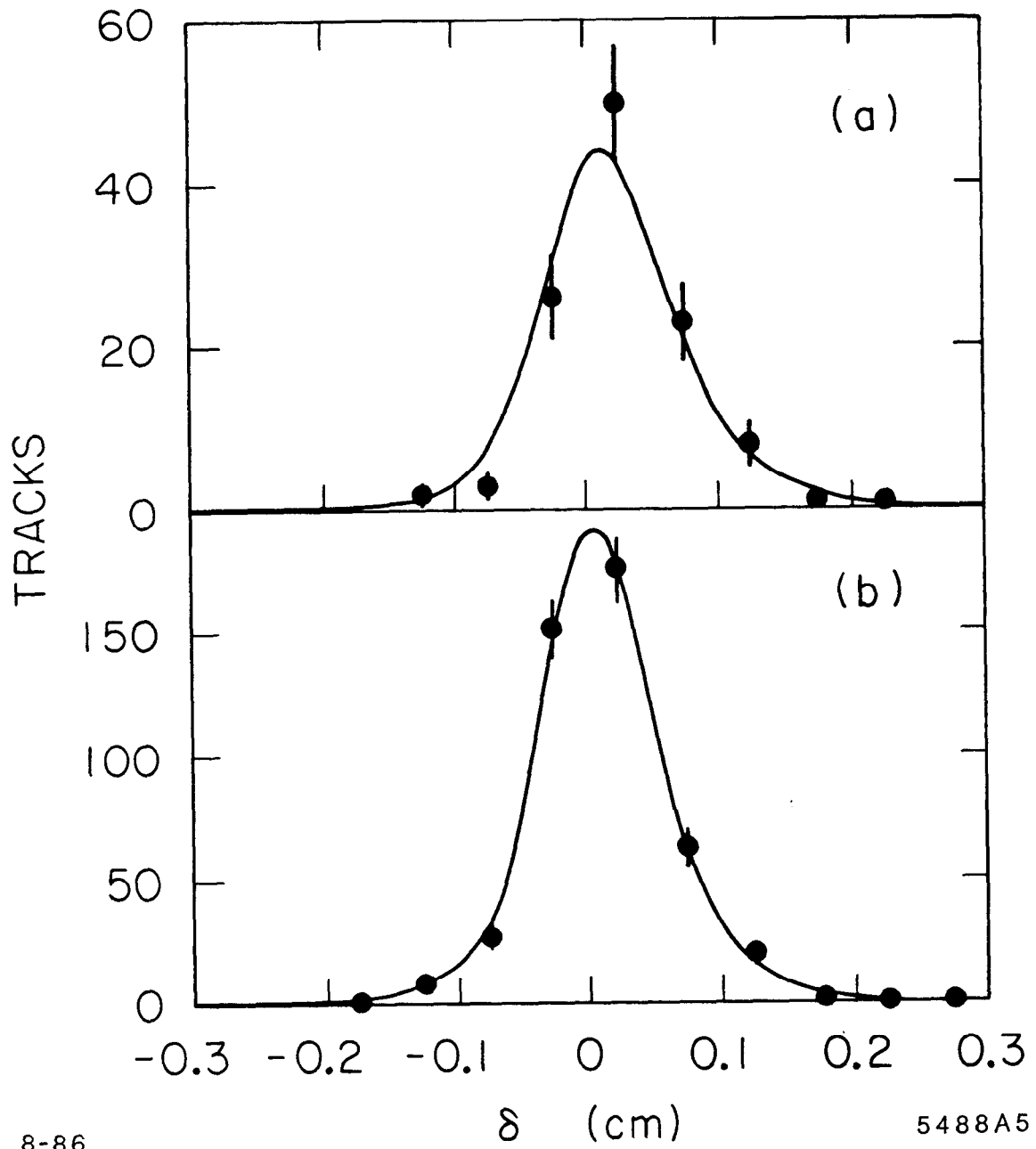


Fig. 3



8-86

5488A5

Fig. 4

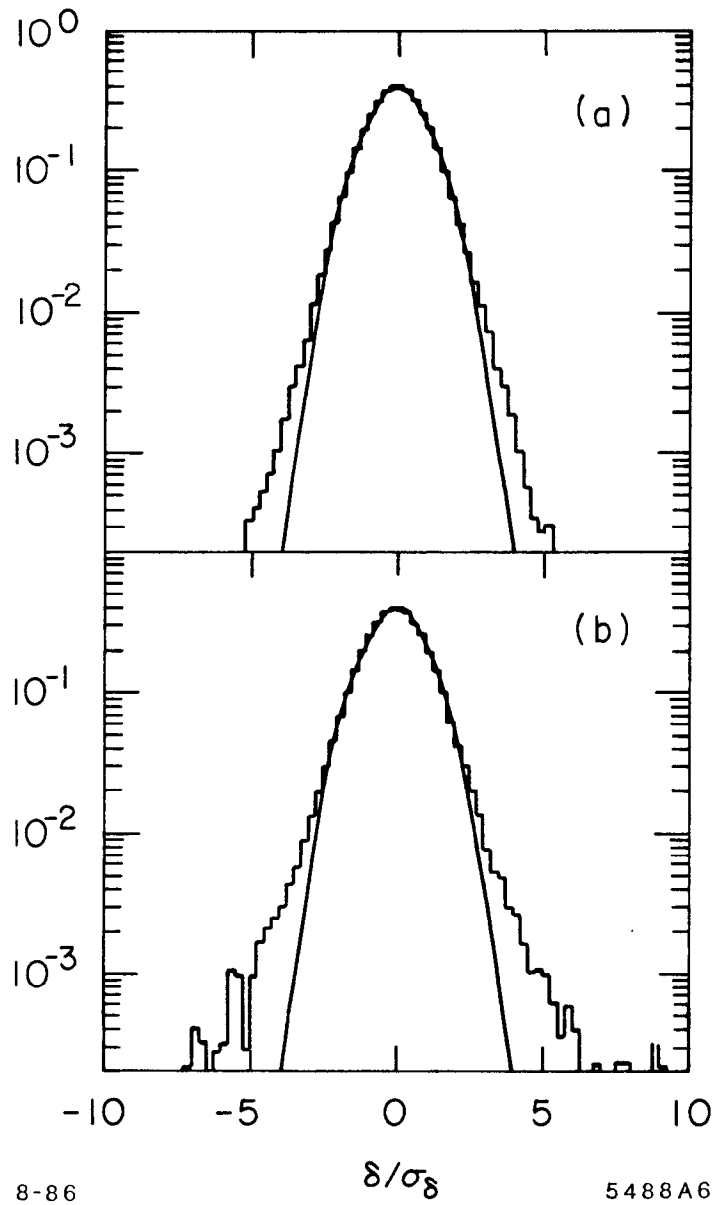


Fig. 5

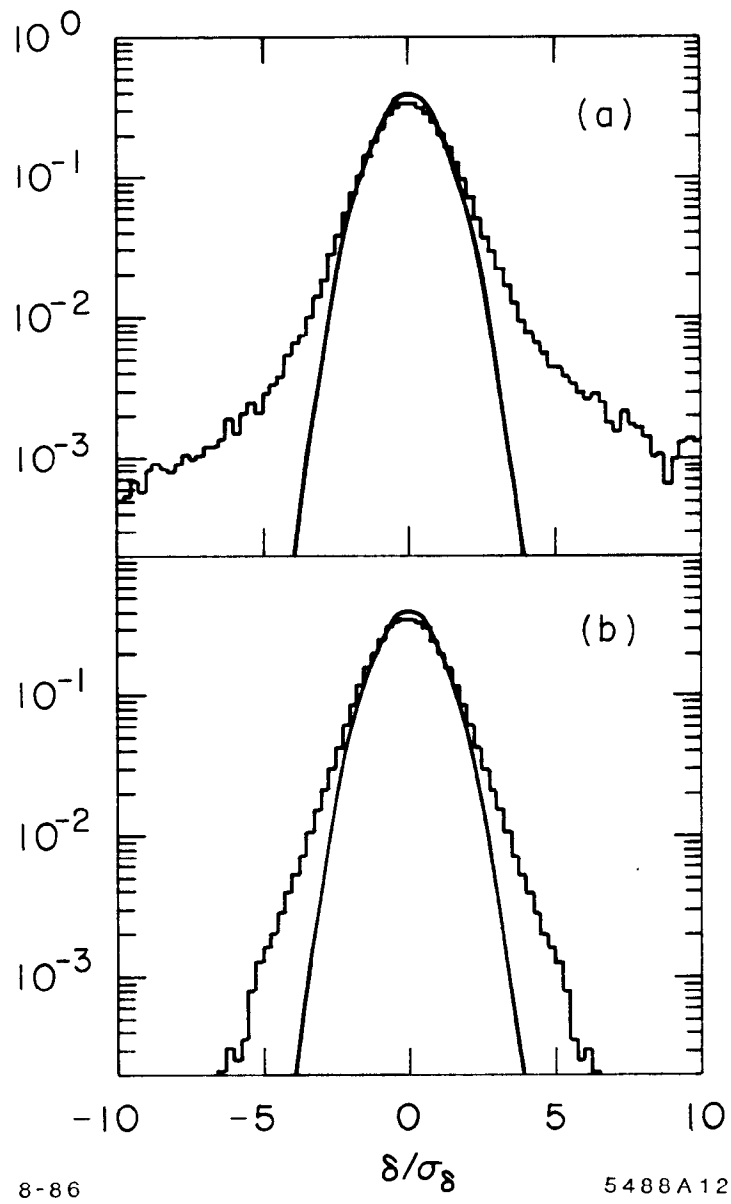


Fig. 6

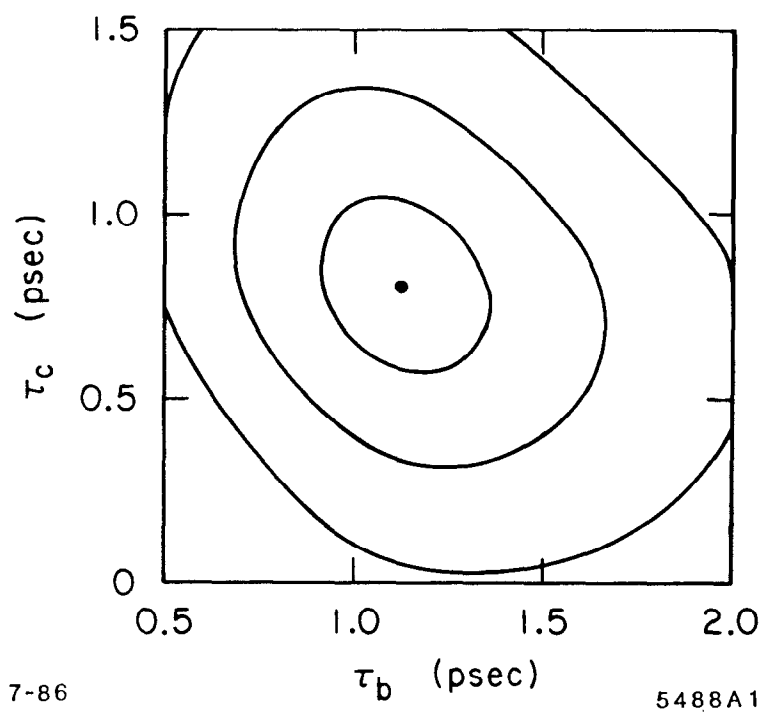


Fig. 7

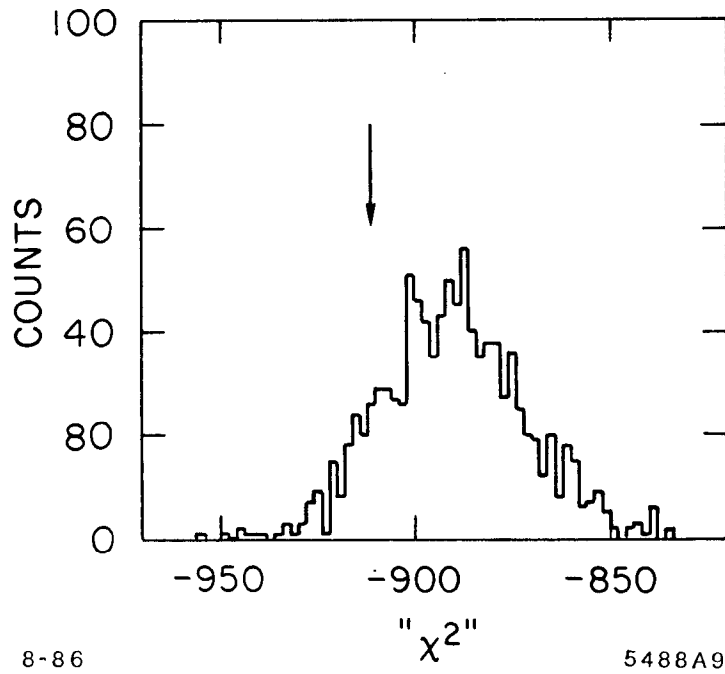


Fig. 8

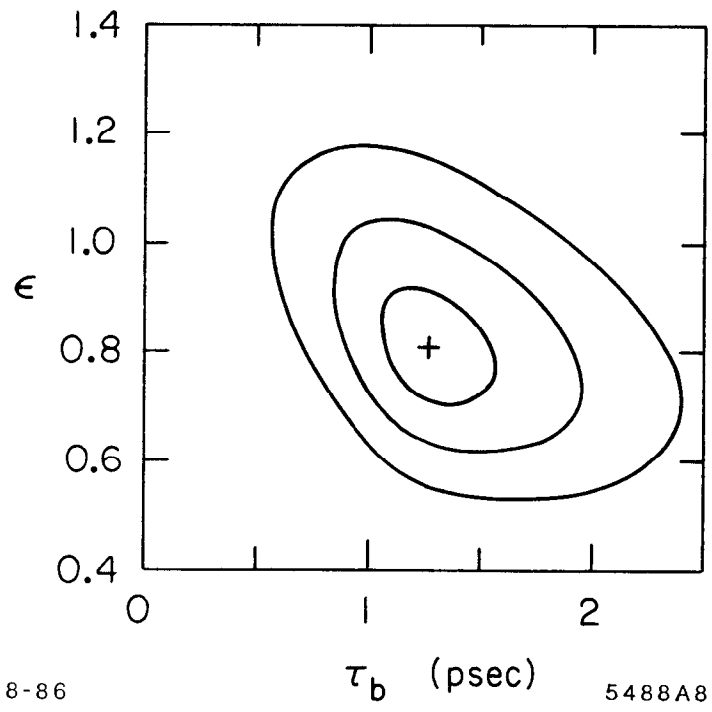
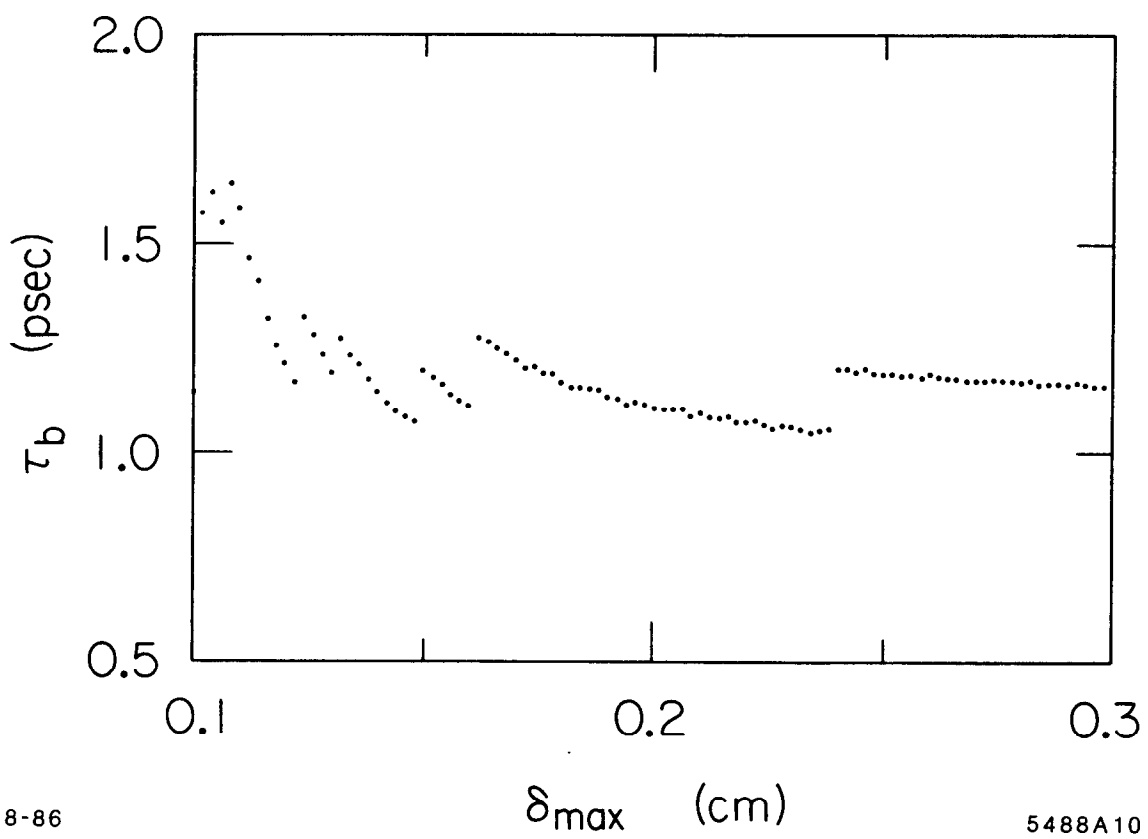


Fig. 9

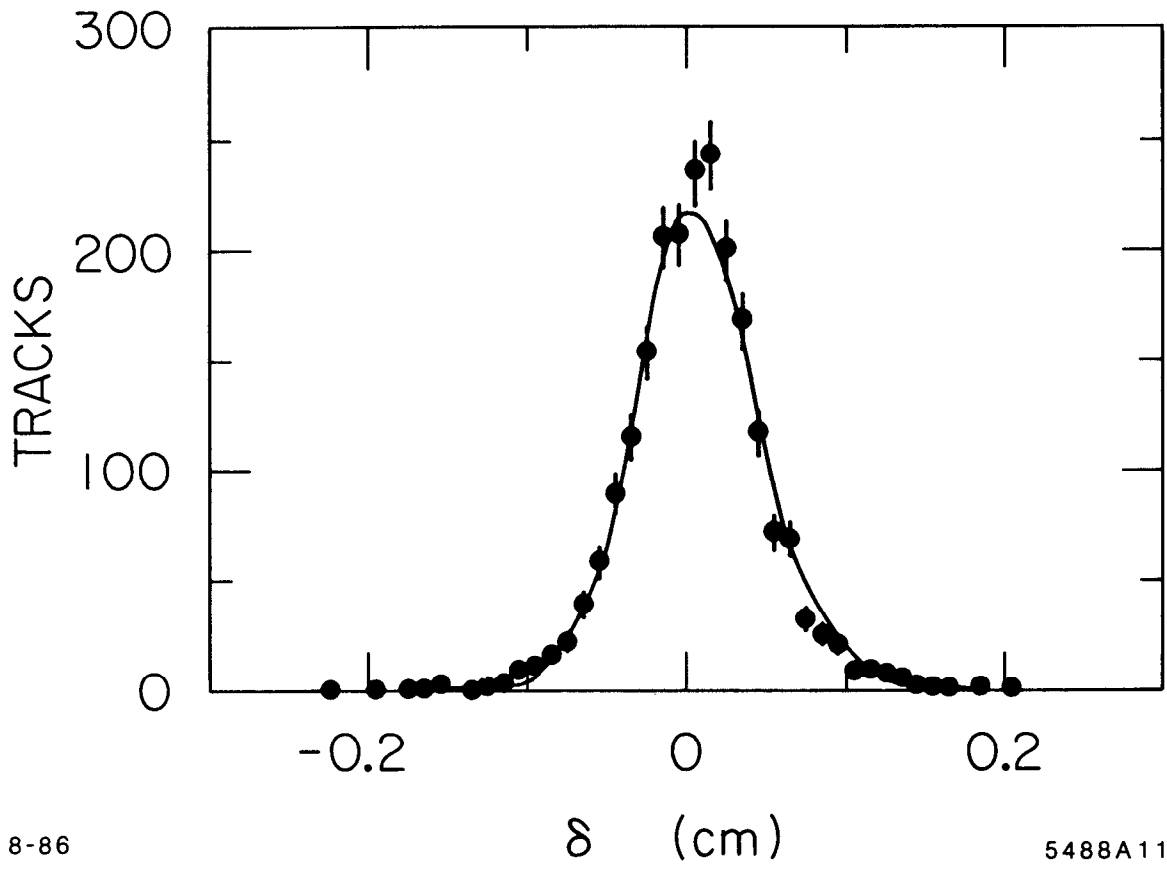


8-86

δ_{\max} (cm)

5488A10

Fig. 10



8-86

5488A11

Fig. 11

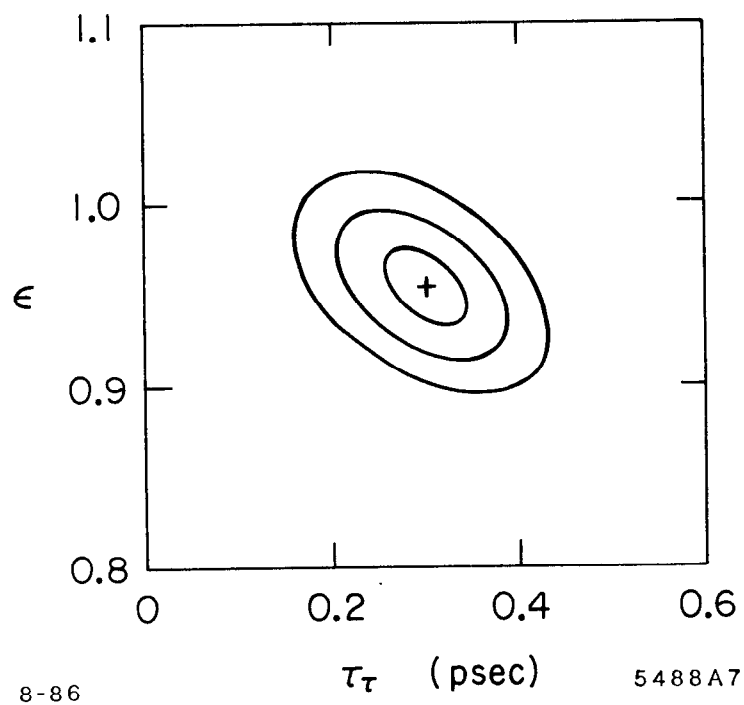


Fig. 12

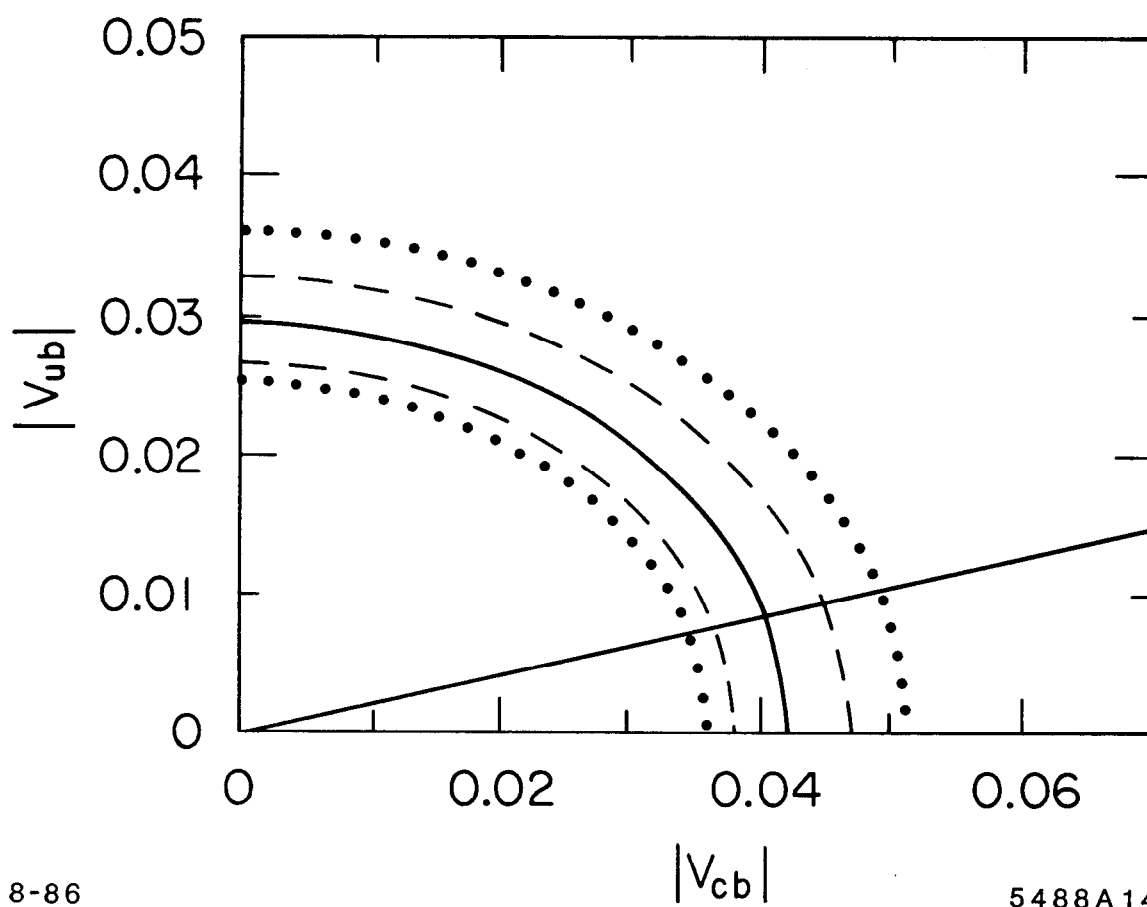
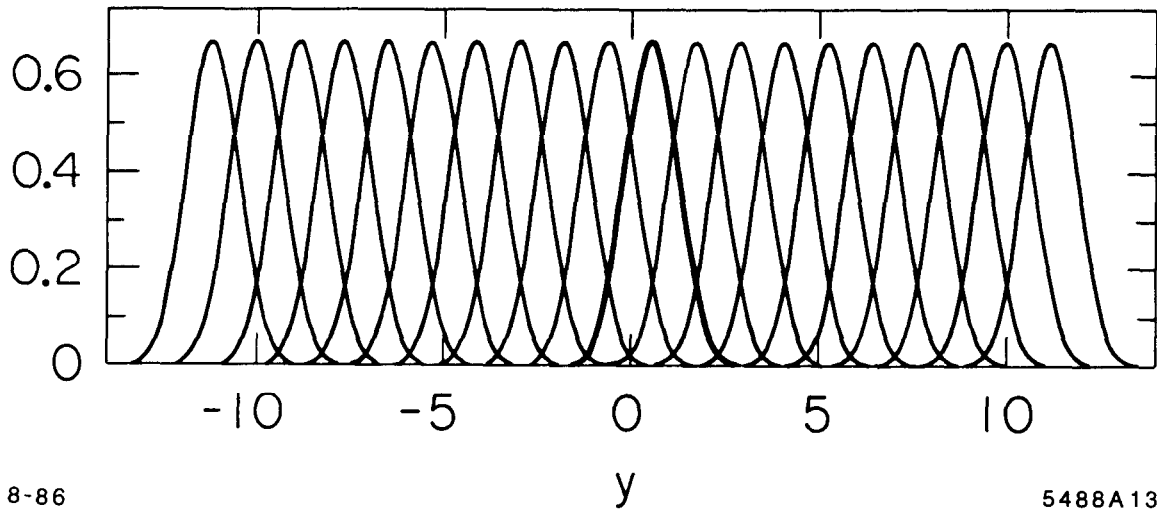


Fig. 13



8-86

5488A13

Fig. 14